Original Article

Molecular dynamics study of ionic diffusion and the FLiNaK salt melt structure

A.Y. Galashev

Institute of High-Temperature Electrochemistry, Ural Branch of Russian Academy of Sciences, Academicheskaya Str., 20, Yekaterinburg, 620990, Russia

A B S T R A C T

In the present work, we carried out a molecular dynamics study of the kinetic properties of the FLiNaK molten salt, as well as a detailed study of the structure of this salt melt. The high value of the self-diffusion coefficient of fluorine ions is due to the large number of Coulomb repulsions between the most numerous negative ions. The calculated values of shear viscosity are in good agreement with the experimental data, as well as with the reference data obtained on the basis of finding the most reliable data. The total and partial functions of the radial distribution are calculated. According to the statistical analysis, fluorine ions have the greatest numerical diversity in the environment of similar ions, and sodium ions with the lowest representation in FLiNaK, have the least such diversity. For the subsystem of fluorine ions, the rotational symmetry of the fifth order is the most pronounced. Some of the fluorine ions form linear chains consisting of three atoms, which are not formed for positive ions. The results of the work give an understanding of the behavior molten FLiNaK under operating conditions in a molten salt reactor and will find application in future studies of this molten salt.

© 2022 Korean Nuclear Society, Published by Elsevier Korea LLC. This is an open access article under the CC BY-NC-ND license (http://creativecommons.org/licenses/by-nc-nd/4.0/).

1. Introduction

Molten fluoride salt FLiNaK can serve as an effective heat carrier at high temperature, low pressure and high radiation fluxes. It can also be used as a coolant or fuel salt for the molten salt reactor (MSR) system [1,2]. Recently, there has again been a significant interest in MSR technology [3,4]. At the same time, priority studies must be carried out in order to determine the structure and composition of the molten salt, which acts as a coolant, both with and without fission products [5]. In this direction, extensive research should be carried out, because more than 50 elements (including fission products, fuel and transuranium elements) can be dissolved in the coolant [6]. At present, FLiBe and FLiNaK are the main candidates for use as a liquid salt reactor coolant. The main advantage of molten fluorides is their stability under radiation conditions. Molten fluorides have higher thermal conductivity values than molten chlorides. In the case of molten salts in the form of mixtures of eutectic composition, the law of simple scaling with respect to changes in density and composition does not hold. A reliable database of FLiNaK properties can be obtained by molecular dynamics (MD) modeling. First-principles molecular dynamics modeling was used to calculate the density, bulk modulus, thermal expansion coefficient, and self-diffusion coefficient FLiNaK and FLiBe [7]. In general, the obtained data are in good agreement with the available experimental data. Molecular dynamics calculations show that the composition of molten LiF-KF mixtures affects the self-diffusion of anions and cations to a lesser extent than temperature [8]. Using computer simulations, it was possible to show that the polarizability of cations and the formation of associates can dictate the mechanism by which the charge is screened in the double electric layer [9]. Although an exhaustive study of the reliability of structural alloys with respect to these salts has not been carried out, it is believed that FLiNaK is inherently more aggressive to structural metals than FLiBe [10].

The purpose of this work is to study in detail the structure of pure molten FLiNaK, which is necessary for the subsequent structural analysis of a more realistic salt melt containing various inclusions.

2. Molecular dynamics

To describe the interaction between ions in the molten salt FLiNaK, the Born-Meyer-Huggins potential was used, the

---

representation of which in the Fumi-Toshi form [11] is:

$$U_{ij}^{tot}(r) = U_{ij}^{rep}(r) + U_{ij}^{disp}(r) + U_{ij}^{q-q}(r) \tag{1}$$

Polarizability effects are not taken into account by this potential. The repulsive part of the potential is given by the expression

$$U_{ij}^{rep}(r) = a_{ij} \bullet b \bullet \exp\left(\frac{\sigma_i + \sigma_j - r}{\rho}\right) \equiv A \bullet \exp\left(\frac{\sigma - r}{\rho}\right) \tag{2}$$

where the total interaction parameter A is determined in terms of the energy parameter b and numerical Pauling coefficients a_{ij} [12]; the parameter σ is determined by the sum of the length parameters (σ_i and σ_j) characterizing the interaction between ions i and j; ρ is the "stiffness" parameter of the ionic system.

The contribution describing the dispersion interaction of the van der Waals type is presented as:

$$U_{ij}^{disp}(r) = -\frac{C_{ij}}{r^6} + \frac{D_{ij}}{r^8} \tag{3}$$

where the coefficient C_{ij} characterizes the dipole-dipole interaction, and the coefficient D_{ij} is introduced to take into account the dipole-quadrupole interaction. These coefficients were obtained by Mayer in quantum mechanical calculations based on experimental data on the absorption of ultraviolet radiation [13].

The Coulomb interaction between ions is given by the contribution U_{ij}^{q-q}

$$U_{ij}^{q-q}(r) = \frac{q_i q_j}{r} \tag{4}$$

where the charges of i and j ions are denoted as q_i and q_j, respectively.

The parameters of the Born-Meyer-Huggins potential for the components of the salt melt FLiNaK can be found in Table 1 of the reference [14].

The self-diffusion coefficient D of atoms was calculated by us from the Einstein relation represented by equation (6). Thus, the value of D was determined from the slope of the dependence of the average square of the displacement $\langle \Delta r^2 \rangle$ of the center of mass of similar atoms on time.

$$\langle \Delta r^2 \rangle = \langle \frac{1}{N} \sum_{i=0}^{N} [r_i(t_0 + dt) - r_i(t_0)]^2 \rangle =$$

$$= \frac{1}{N \bullet n_t} \sum_{i=0}^{N} \sum_{j=0}^{n_t} [r_i(t_j + dt) - r_i(t_j)]^2 \tag{5}$$

where N is the number of atoms of a certain sort, n_t —is the number of intervals for determining $\langle \Delta r^2 \rangle$, t_0 and t_j — are the initial times, angle brackets denote averaging over selected equally spaced time points.

$$D = \frac{1}{6} \lim_{t \to \infty} \langle \Delta r^2 \rangle \Big/ t \tag{6}$$

The MD calculation of shear viscosity is based on the use of the Einstein relation [15]:

$$\eta = \lim_{t \to \infty} \frac{1}{2t} \frac{V}{k_B T} \langle \left(\int_0^t P_{\alpha\beta}(\tau) d\tau \right)^2 \rangle \tag{7}$$

where $P_{\alpha\beta}$ represents the off-diagonal components of the stress tensor (i.e., P_{xy}, P_{xz}, and P_{yz}), k_B is the Boltzmann constant, t is the correlation time, and V and T are the volume and temperature of the system, respectively.

The partial function of the radial distribution is defined as

$$g_{\alpha\beta} = \frac{dn_{\alpha\beta}(r)}{4\pi r^2 dr \rho_\alpha} \tag{8}$$

where $dn_{\alpha\beta}(r)$ is number of atoms of sort β in a shell dr at the distance r of atom of sort α, partial density of species α: $\rho_\alpha = \frac{V}{N_\alpha} = V/(N x_\alpha)$, x$\alpha$ represents the concentration of atomic species α.

The first coordination number is defined as [16].

$$n_{\alpha\beta} = 4\pi\rho x_\beta \int_0^{r_{min}} r^2 g_{\alpha\beta}(r) dr \tag{9}$$

where ρ is the number density, x_β is the concentration (N_β/N) of species β, r_{min} is the first minimum of the $g_{\alpha\beta}(r)$ function.

The hydrodynamic radius is a characteristic of the diffusing object. The hydrodynamic radius can be calculated from the Stokes-Einstein correlation between the self-diffusion coefficient and the shear viscosity [17].

$$R_h = \frac{k_B T}{6\pi\eta D} \tag{10}$$

where, D is the self-diffusion coefficient; η is the viscosity; T is temperature; and k_B is the Boltzmann constant. Sometimes, instead of 6, 4 is used in the denominator of expression (10), but for ions of different sizes experiencing Coulomb interactions it is better to use the value 6, as in the case of a model of rough objects [21].

Molten FLiNaK was prepared from 20000 ions by melting superheated fcc crystals: LiF (9300 ions), NaF (2300 ions) and KF (8400 ions) at 3000 K for 1 million time steps ($\Delta t = 0.1$ fs). This composition of the system corresponded to the FLiNaK eutectic: LiF - 46.5-mol%, NaF - 11.5-mol% and KF - 42.0-mol%. The melt was then held at this temperature for 2 million Δt for complete mixing. The above procedures were performed in the NVT ensemble. The next stage of system preparation consisted in bringing the melt to the required initial density and temperature of 800 K and holding the system under these initial conditions. The total duration of the

Table 1
The location of the first maximum and the first coordination number determined from the partial radial distribution functions[a].

Element		$r_{\alpha\beta}$			$n_{\alpha\beta}$		
α	β	MD	*Ab initio* MD	Experiment	MD	*Ab initio* MD	Experiment
Li	F	1.60	1.60	1.83	3.3	3.6	3.3
Na	F	2.05	2.20	2.18	4.2	4.9	3.8
K	F	2.55	2.75	2.59	5.2	6.9	4.0
F	F	2.85	2.85	3.05	9.1	—	8.9

[a] MD, $T = 800$ K, the work presented here; ab initio MD, $T = 973$ K, [26]; Experiment, $T = 793$ K, [25].

calculation was 3 Δt. These and subsequent calculations were performed in the NPT ensemble. All calculations at temperatures above 800 K were carried out sequentially by increasing the temperature by a given value of ΔT, followed by holding at a new temperature (0.5 million Δt) and performing the main calculation with a duration of 2 million Δt at each temperature. To expand the system, periodic boundary conditions were imposed on the main MD cell. Long-range interactions were determined based on the Particle-Particle Particle-Mesh (PPPM) summation method [18], i.e. the charges were placed on a 3D grid and the Fastest Fourier Transform was used to solve the Poisson equations. Electric fields were interpolated from grid points back to charged particles.

Traditionally, the structure of a liquid is represented by a radial distribution function, and the structure of a multicomponent liquid is represented by a set of partial radial distribution functions. However, in both cases, the three-dimensional structure is represented as a one-dimensional function, as a result of which a significant part of the information is lost. A more accurate three-dimensional representation of the structure of a liquid can be performed by the method of statistical geometry based on the construction of Voronoi polyhedra (VP). VP is constructed by drawing planes perpendicular to the segments connecting the central atom with its nearest neighbors. Moreover, these planes are drawn through the midpoints of these segments. The constructed polyhedron is convex and no point in space can be simultaneously closer to two centers of the system of polyhedra. With such a partitioning, the polyhedra densely (without voids) fill the entire space, and the partitioning is uniquely determined by the system of the central points (i.e., atoms). Usually the structure of the considered system (liquid) is interpreted with the help of statistical distributions of the constructed polyhedra. Such distributions can be distributions of polyhedra by the number of faces, distributions of faces by the number of sides they contain, distributions of the lengths of the segments connecting geometric neighbors (which form VP faces), angular distributions of nearest geometric neighbors, and some other characteristics. To construct the angular distributions, we consider the angles θ enclosed between pairs of segments connecting the center VP with geometric neighbors. In other words, the vertex of the angle θ coincides with the center of VP, and the sides are perpendicular to the corresponding faces. Representation of the structure by constructing Voronoi polyhedra makes it possible to fully reflect its three-dimensional nature. VPs were built every 10,000 time steps, so that during a calculation with a duration of 1 million time steps for a system containing 20,000 ions, 2 million polyhedra were built.

3. Results

The calculated self-diffusion coefficients D along with the experimental values of D [19] of the F^-, Li^+, Na^+ and K^+ ions in molten FLiNak are shown in Fig. 1. As can be seen from the Figure, the calculated and experimental values of D for Li^+ and Na^+ ions agree on average within 22%, and for K^+ and F^- ions, within 12%. The D coefficients of the ions forming FLiNaK increase with increasing temperature. The behavior of the $D(T)$ function can be approximated using a linear relationship also shown in the figure. In addition, Fig. 1 shows the analytical expression of the obtained approximation dependence $D(T)$. The D values for all the ions under consideration are not very different. The highest values of D were obtained for F^- ions, and not for the lightest Li^+ ions, which can be explained by their highest abundance in the salt melt. Their share is 2.15 times greater than the number of the second largest number of Li^+ ions. The sign of the ion charge also affects the mobility. F^- ions are the only particles in the system that carry a negative electrical charge. Note that in the eutectic FLiNaK studied by us the number

and total charges of positive and negative ions are the same. However, the total mass of ions carrying a positive electric charge exceeds the total mass of ions (F^-) with a negative charge 1.17 times. Among the positive ions, K^+ ions show the highest mobility, and Li^+ ions show the lowest. Exactly the same relationship between the D coefficients for ions was obtained in ab initio MD simulations of pure FLiNaK at temperatures of 973 K and 1223 K [7]. The D coefficient for F^- ions still dominates even at 1423 K. The mechanism of diffusion in this molten salt is still unknown.

Fig. 2 shows the temperature dependences of the shear viscosity $\eta(T)$ of pure FLiNaK, obtained in experiment [20–22] and in MD calculations [23], including the data of this work. In Ref. [26], the most important data for the shear viscosity of pure FLiNaK were analyzed. After a critical study, new improved reference viscosity correlations were recommended. The dependence $\eta(T)$ calculated by us agrees well with the corresponding curve obtained in a recent experiment performed using a rheometer FRS-1600 [22], as well as with the values of dynamic viscosity recommended in Ref. [24].

Molten salts have a low viscosity. This ensures good mixing of the ions of which they are composed. Small discrepancies between the force fields defined in classical ion dynamics by interaction potentials can disrupt the short-range order for ions, which will lead to a change in the structural and kinetic characteristics. In other words, the structural properties and dynamic viscosity of molten salts are sensitive to the details of the force field. The closeness of the calculated data on shear viscosity with the experimental data for η in a wide temperature range indicates an adequate selection of all interaction potentials.

The hydrodynamic radii of the FLiNaK salt melt increase with increasing temperature (Fig. 3), just as in the case of the molten LiCl−NaCl−KCl system [24]. This is due to the rapid decrease in the shear viscosity of the molten FLiNaK with increasing temperature. In this case, the self-diffusion coefficient plays a secondary role, determining only the nature of the change of R_h in a given temperature range. The initial value of R_h for Na^+ ions is higher than for other ions, because sodium ions are characterized by a lower initial coefficient of self-diffusion. If the increase in the R_h value for Li^+, K^+ and F^- ions is almost linear, then the increase in this characteristic for Na^+ ions follows a different path than the linear change. The reason for this may be the lowest concentration of Na in FLiNaK relative to the concentration of other elements, which contributes to greater variability in the nature of the change in the kinetic properties of the Na subsystem.

Fig. 4 shows the total experimental and partial calculated radial distribution functions for molten pure FLiNaK. As can be seen from the upper parts of Fig. 4, the experimental function $g(r)$ [25] can be represented by the composition of the partial functions $g_{F-F}(r)$ and $g_{K-F}(r)$, i.e. it can be formed from partial RDFs related to heavy ions in FLiNaK. In other words, when constructing this function, the diffraction of X-rays by F^- and K^+ ions was mainly taken into account. In general, the partial RDFs determined in the MD calculation are in good agreement with the corresponding functions obtained in the ab initio MD calculation [26]. Quantification of the RDFs can be done by the location value $r_{\alpha\beta}$ of the first maximum and by the first coordination number $n_{\alpha\beta}$ determined from these functions. The calculated and experimental values of $r_{\alpha\beta}$ and $n_{\alpha\beta}$ are presented in Table 1.

The MD calculation data and experimental data [25] are presented here at almost the same temperatures, while the ab initio molecular dynamics data [26] are given at a higher temperature. Moreover, the value of $n_{\alpha\beta}$, determined through the function $g_{F-F}(r)$, is missing in Ref. [26]. The $r_{\alpha\beta}$ values obtained from the X-ray diffraction data turn out to be slightly higher than the corresponding values found using the MD calculation. However, most of the values of $n_{\alpha\beta}$ determined in the experiment are lower than the
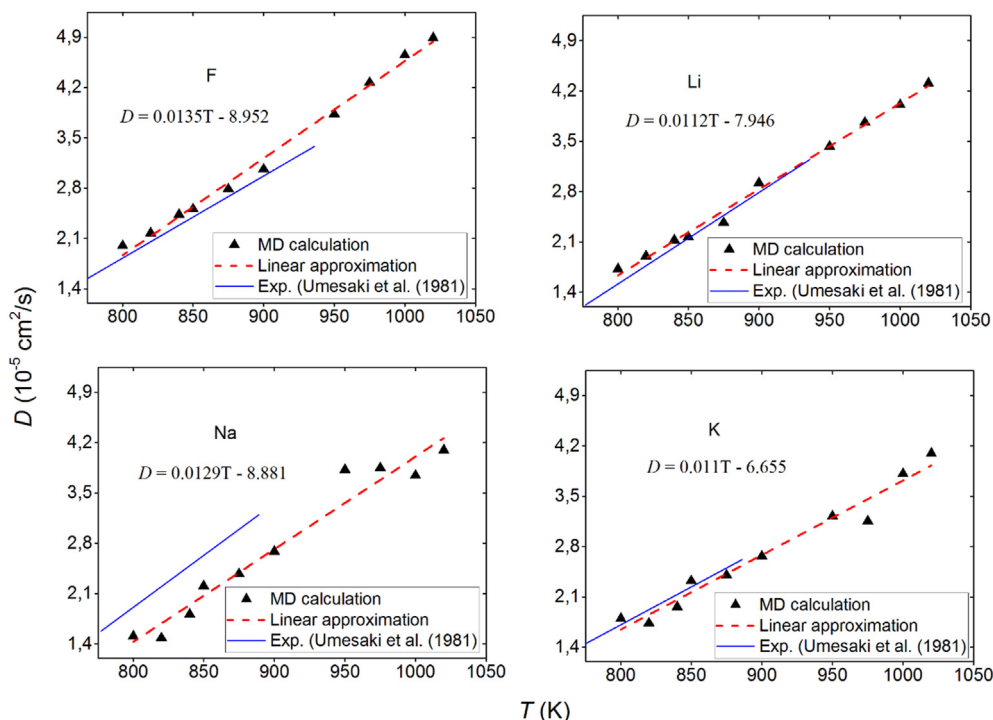
Fig. 1. Self-diffusion coefficients of pure FLiNaK components; the linear approximation of the MD calculation is presented as a dotted line and an analytical expression; experimental results are taken from Ref. [19].
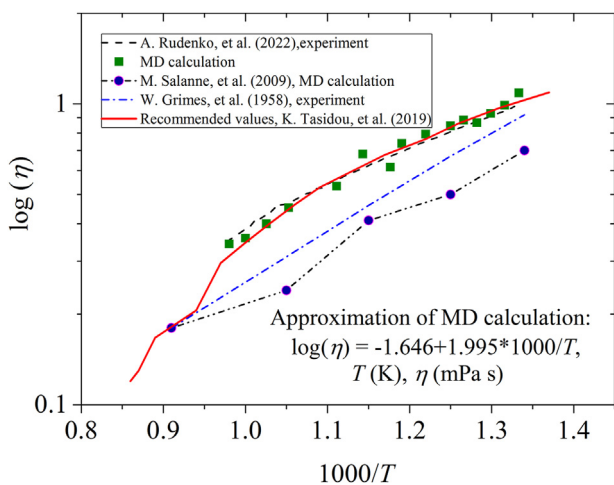

Fig. 2. Shear viscosity of molten salt FLiNaK, obtained both in experiment and MD simulation; the linear approximation of the MD results is also represented; shear viscosity is expressed in mPa·s.

Fig. 3. Temperature dependence of hydrodynamic radii of cations and anions.

coordination numbers calculated by the MD method. The exception is the case indexed as Li−F, where the calculated value of $n_{\alpha\beta}$ is equal to the experimental value. Note that the coordination number, defined by the index Me−F, where Me = Li, Na, or K, increases in the same order as the radius of the alkali metal ion, i.e. from Li to K.

The calculated temperature dependence of the coordination numbers characterizing the structure of FLiNaK is shown in Fig. 5. With an increase in temperature, a decrease in all coordination numbers is observed, which can range from 3% to 10% over the entire temperature range. The most significant temperature changes in the coordination number $n_{\alpha\beta}$ occur for the cases
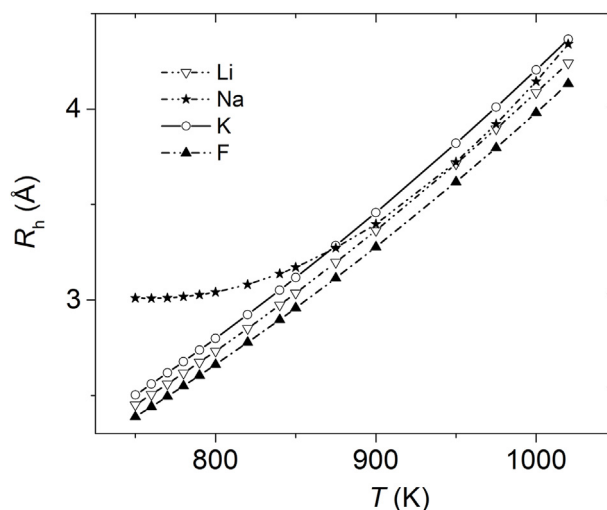
$\alpha = \beta = $ Li and $\alpha = \beta = $ F, i.e. for the cation having the highest self-diffusion coefficient among cations and for the anion (with the highest D value). The coordination number calculated through the partial radial distribution function is directly proportional to the concentration x_{β} of component β (see formula 9). When the x_{β} concentration becomes too low (as is the case for the Na concentration in FLiNaK), the spherical approximation used to determine the probability of finding a near neighbor becomes unsatisfactory. In other words, a spherical layer of thickness dr may not include geometric neighbors whose arrangement does not satisfy spherical symmetry. A significant increase in dr will lead to a serious decrease in the accuracy of the definition of the function $g_{\alpha\beta}(r)$, and as a consequence of r_{min}, i.e. the upper limit of the integral in
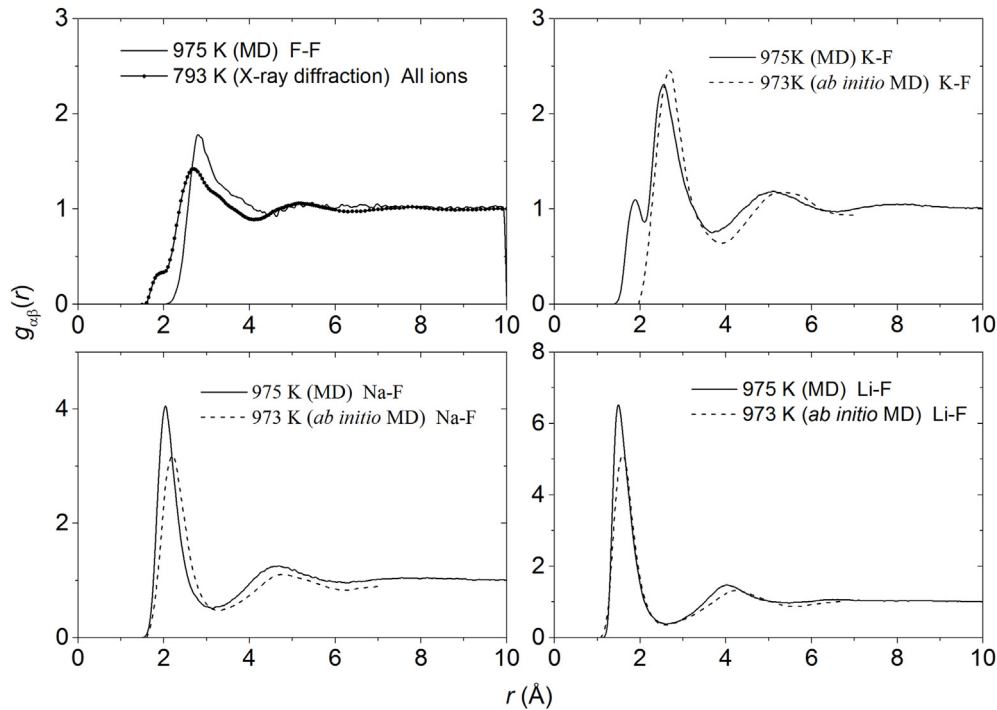
Fig. 4. Total experimental radial distribution function (873 K) [25] and partial RDFs calculated by molecular dynamics (MD, present work, 975 K) and ab initio molecular dynamics (ab initio MD, 973 K) [26] methods.

expression (9). Thus, at a low concentration x_β, the determination of the coordination number through the function $g_{\alpha\beta}(r)$ becomes incorrect. Therefore, the value of $n_{\alpha\beta}$ ($\alpha = \beta = Na$) is not shown in Fig. 4. It was also not defined in Refs. [25,26].

Let us now consider the mutual arrangement of ions of the same kind using the method of statistical geometry. The distributions of polyhedra by the number of faces (n distributions) for the Li, Na, K and F subsystems are shown in Fig. 6. As can be seen from the figure, the most representative is the n distribution for the F subsystem, and the poorest in relation to the variety of face types in VPs is the n distribution for the Na subsystem. The number of F⁻ ions is equal to the number of all positive ions (Li⁺, Na⁺ and K⁺) taken together and is 8.7 times greater than the number of Na⁺ ions, which are the least in the system. There are 1% more Li⁺ ions in the system than K⁺ ions, and the n distribution for the Li subsystem has a slightly larger representation than that for the K subsystem. Li⁺ ions are mostly surrounded by 4—6 same-type ions, Na⁺ and K⁺ ions are surrounded predominantly by 4 of the same ions (Na⁺ and K⁺), and F⁻ ions have a wide spectrum of the same type environment with a maximum at $n = 11$.

The distribution of faces according to the number of sides (m distribution) shows which rings of the same type of ions are visible to an observer located at the center of a given VP. As can be seen from the inserts in Fig. 6, for the most numerous F⁻ and Li⁺ ions in the system, the maximum of the m distribution is localized at $m = 5$. The localization of the m distribution maximum for the less numerous K⁺ and Na⁺ ions fall on $m = 4$ and 3, respectively. The widest m spectrum is observed for the F subsystem, and the Na subsystem has the poorest m spectrum.

The shape of the angular distribution of the nearest geometric neighbors is unique for the subsystem of each type and reflects the special type of mutual arrangement of the same type ions (Fig. 7). The bimodal θ distribution for the Li subsystem is characterized by a low and rather narrow first peak. For the Na subsystem, the distribution has one pronounced peak and a shoulder to the right of it. The bimodal θ distribution for the K subsystem has a nonzero intensity only at angles $\theta > 30°$. The first peak in this distribution is higher than the second peak. In the case of the F subsystem, the θ distribution consists of two parts: a sharp peak near 0° and a wide part of the θ spectrum, which has a small deflection in the vicinity of the angle 72°. Only for the F subsystem the θ distribution has a pronounced non-zero intensity at $\theta = 0°$. This means that three F⁻ ions can lie in a straight line, which is almost never the case for positively charged ions.
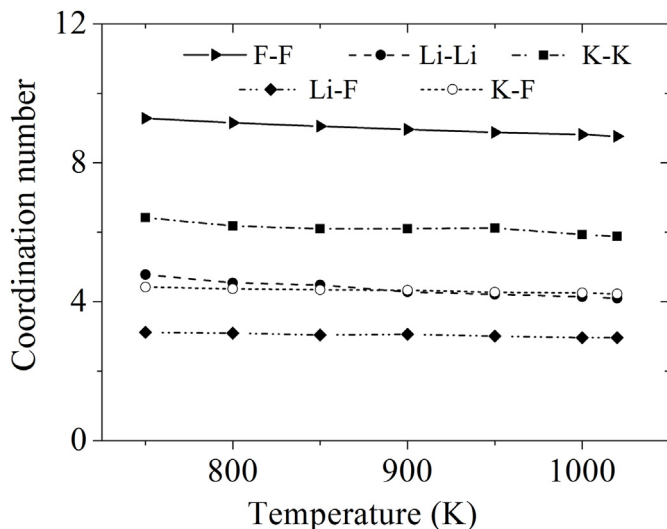

Fig. 5. Temperature dependence of the first coordination numbers of the molten FLiNaK salt.
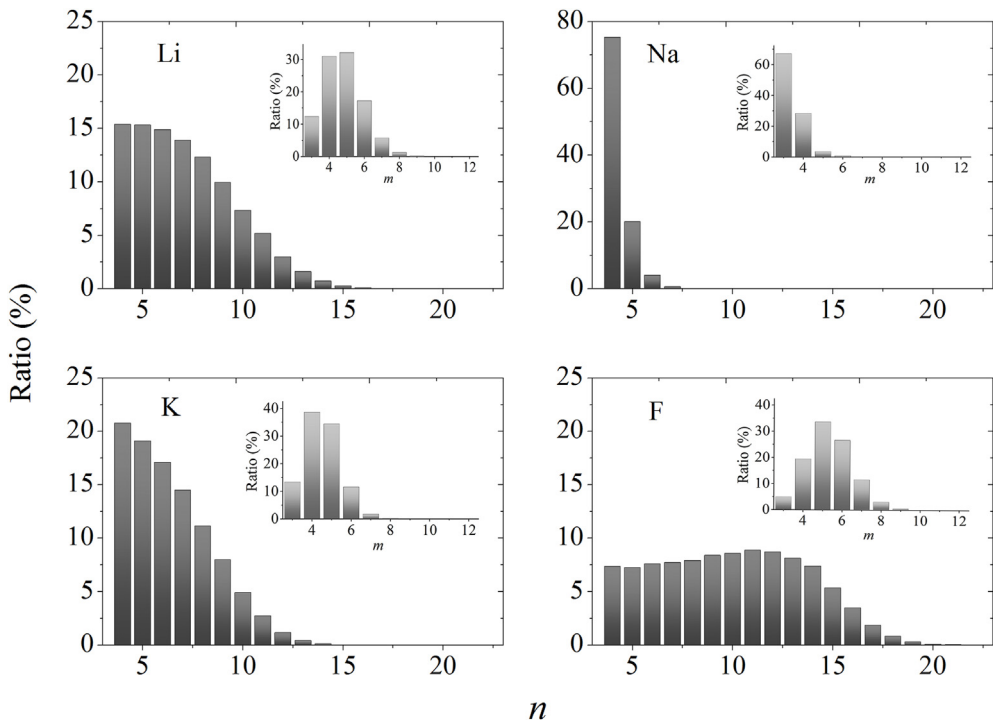
Fig. 6. The distribution of Voronoi polyhedra by the number of faces for the Li-, Na-, K- and F- subsystem of pure FLiNaK at a temperature of 975 K; in insets: distribution of faces by the number of sides corresponding to each n distribution.
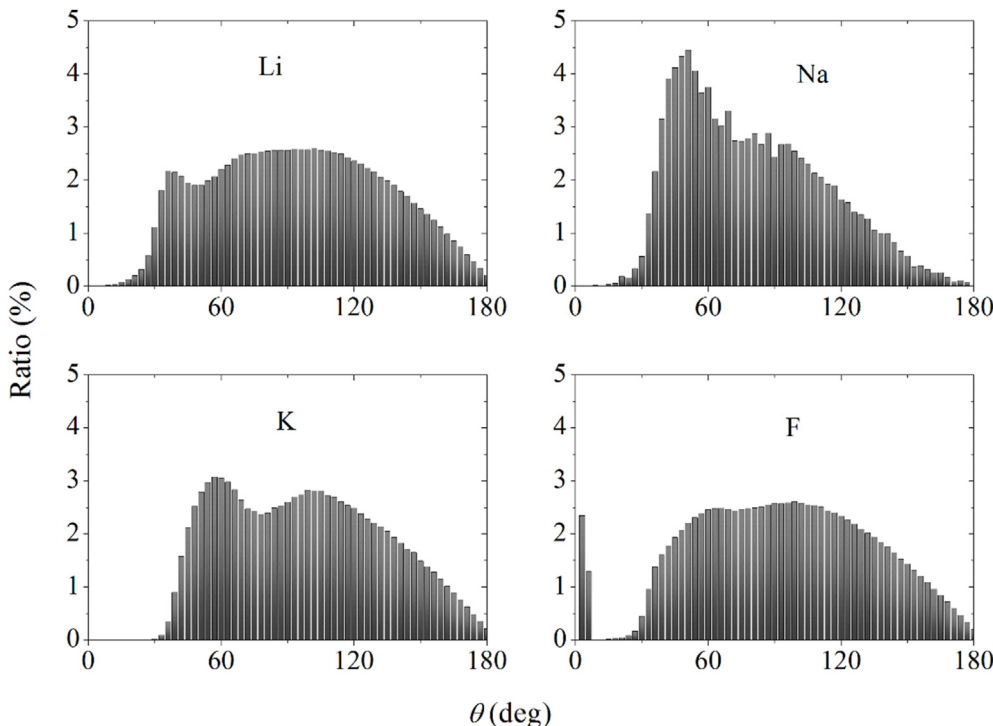

Fig. 7. Angular distributions of nearest geometric neighbors for the Li-, Na-, K- and F- subsystem of pure FLiNaK at 975 K.

4. Discussion

Knowledge of the structural and kinetic characteristics of molten salts makes it possible to increase the efficiency of energy conversion for electricity production and to diversify the energy products produced by nuclear reactors. In addition, these data help to simplify the implementation of high reactor safety standards, facilitate the demonstration of the safety of developed reactors, and improve economic performance [27–29].

The self-diffusion coefficient is an important transport property

of the salt melt. Experimental methods for determining D face significant difficulties, among which are the uncertainty in establishing such characteristics as the number of electrons transferred in the electrode reaction, the electrode area, the volume concentration of electroactive particles, and the chemical instability of the structural materials used at high temperatures [30].

The actual calculations show that, in the operating temperature range, the self-diffusion coefficients for F^- ions are higher than the values of the D coefficient for Li^+ ions. This may be due to the fact that the most numerous F^- ions in the system have significantly more repulsive interactions in the specific ratio than any other ions, which mainly tend to be surrounded by negative ions, i.e. F^-. Calculation of hydrodynamic radii for various components of molten FLiNaK shows that there is a possibility that the diffusion mechanism in multicomponent molten salts involves complexation.

The discrepancy between the calculated structural characteristics and the experimental data may be due to the inaccuracy of processing the diffraction data for molten salts [31]. In this case, a low signal-to-background ratio and a rapid decrease in the scattering intensity with increasing wavenumber (q) are observed. It is difficult to obtain the exact value of the structure factor $S(q)$ at large q. This entails inaccuracy in the determination of RDF and coordination number.

Various methods have been used to predict the structure and physical properties of FLiNaK, including machine learning neural network force field [32]. However, a detailed three-dimensional structure of molten FLiNaK has not yet been presented. In this work, using the method of statistical geometry based on the construction of Voronoi polyhedra, we study the mutual arrangement of ions of the same type in the molten FLiNaK salt. Among the considered ionic subsystems in this molten salt, the appearance of a five-link rings of F^- ions (see m distribution) is the most pronounced. This means that the subsystem consisting of F^- ions has the closest to the liquid mutual arrangement of ions [33,34], which is consistent with the higher mobility of these ions in the system. The main part of the angular distribution of the nearest geometric neighbors for the F^- ion subsystem is represented by a dome with a very weak expression of bimodality, which is characteristic of a high degree of disorder with an almost complete absence of short-range order. At the same time, the subsystem of fluorine ions is the only subsystem in which a peak appeared in the angular distribution in the vicinity of the angle $\theta = 0°$. The appearance of this angle means that a certain part of the F^- ions can form triplets of ions lying on the same straight line. It is obvious that such a possibility can exist if there is a large freedom for the appearance of various packings from single-sorted ions. And this happens because the most numerous F- ions form in FLiNaK a subsystem with the greatest variety of ion packings.

5. Conclusion

In this work, the diffusion characteristics, shear viscosity and detailed structure of the eutectic salt melt FLiNaK in the operating temperature range of the liquid salt reactor are determined by the molecular dynamics method. It is shown that the temperature dependence of the self-diffusion coefficient for the same-type ions contained in this molten salt can be represented by a linear dependence. In a wide temperature range, the calculated shear viscosity agrees with the reference experimental values of this quantity. Due to the high concentration of F^- ions and, therefore, the stronger Coulomb repulsion, these ions have the highest mobility in the salt melt. The main peaks of the partial radial distribution functions $g_{Me-F}(r)$ strongly decrease their intensity and shift towards larger distances upon transition from a lighter metal

(Li) to a heavier one (K). F^- ions have the greatest diversity in the number of diverse geometric neighbors, and the most sparsely represented Na^+ ions have the most poor quantitative composition of the environment. The subsystem of F^- ions is distinguished by the most pronounced feature of the liquid structure - the rotational symmetry of the fifth order. In the angular distribution of the nearest geometric neighbors for this subsystem, a peak appears in the vicinity of the angle $\theta = 0°$, and the main part of the θ spectrum has an almost unimodal shape.

The results obtained in this work will facilitate the screening of molten salts used in molten salt reactors.

Declaration of competing interest

The authors declare that they have no known competing financial interests or personal relationships that could have appeared to influence the work reported in this paper.

Appendix A. Supplementary data

Supplementary data to this article can be found online at https://doi.org/10.1016/j.net.2022.12.029.

References

[1] P.N. Haubenre, J.R. Engel, Experience with the molten-salt reactor experiment, Nucl. Appl. Technol. 8 (1970) 118−136.

[2] M.W. Rosenthal, P.R. Kasten, R.B. Briggs, Molten-salt reactors—history, status, and potential, Nucl. Appl. Technol. 8 (1970) 107−118.

[3] L. Mathieu, D. Heuer, R. Brissot, C. Garzenne, C.L. Brun, D. Lecarpentier, E. Liatard, J.-M. Loiseaux, O. Meplan, E. Merle-Lucotte, A. Nuttin, E. Walle, J. Wilson, The thorium molten salt reactor: moving on from the MSBR, Prog. Nucl. Energy 48 (2006) 664−679.

[4] S. Delpech, E. Merle-Lucotte, D. Heuer, M. Allibert, V. Ghetta, C. Le-Brun, X. Doligez, G. Picard, Reactor physic and reprocessing scheme for innovative molten salt reactor system, J. Fluor. Chem. 130 (2009) 11−17.

[5] B.A. Frandsen, S.D. Nickerson, A.D. Clark, A. Solano, R. Baral, J. Williams, J. Neuefeind, M. Memmott, The structure of molten FLiNaK, J. Nucl. Mater. 537 (2020), 152219.

[6] P. Soucek, F. Lisý, R. Tulackova, J. Uhlír, R. Mraz, Development of electrochemical separation methods in molten LiF-NaF-KF for the molten salt reactor fuel cycle, J. Nucl. Sci. Technol. 42 (12) (2005) 1017−1024.

[7] H.O. Nam, A. Bengtson, K. Vurtler, S. Saha, R. Sakidja, D. Morgan, First-principles molecular dynamics modeling of the molten fluoride salt with Cr solute, J. Nucl. Mater. 449 (2014) 148−157.

[8] V. Sarou-Kanian, A.-L. Rollet, M. Salanne, P.A. Madden, Diffusion coefficients and local structure in basic molten fluorides: in situ NMR measurements and molecular dynamics simulations, Phys. Chem. Chem. Phys. 11 (48) (2009) 11501−11506.

[9] L. Langford, N. Winner, A. Hwang, H. Williams, L. Vergari, R.O. Scarlat, M. Asta, Constant-potential molecular dynamics simulations of molten-salt double layers for FLiBe and FLiNaK, J. Chem. Phys. 157 (2022), 094705.

[10] S. Guo, J. Zhang, W. Wu, W. Zhou, Corrosion in the molten fluoride and chloride salts and materials development for nuclear applications, Prog. Mater. Sci. 97 (2018) 448−487.

[11] M.P. Tosi, F.G. Fumi, Ionic sizes and born repulsive parameters in the NaCl-type alkali halides—II: the generalized Huggins-Mayer form, J. Phys. Chem. Solid. 25 (1964) 45−52.

[12] L. Pauling, The molecular structure of the tungstosilicates and related compounds, J. Am. Chem. Soc. 51 (1929) 2868−2880.

[13] J.E. Mayer, Dispersion and polarizability and the van der Waals potential in the alkali halides, J. Chem. Phys. 1 (1933) 270−279.

[14] D.J. Adams, I.R. McDonald, Rigid-ion models of the interionic potential in the alkali halides, J. Phys. C Solid State Phys. 7 (1974) 2761−2775.

[15] K. Meier, A. Laesecke, S. Kabelac, Transport coefficients of the Lennard-Jones model fluid. I. Viscosity, J. Chem. Phys. 121 (2004) 3671−3687.

[16] B.B. Karki, D. Bhattari, L. Stixrude, First-principles calculations of the structural dynamical, and electrical properties of liquid MgO, Phys. Rev. B 73 (2006), 174208.

[17] J.A. Armstrong, P. Ballone, Computational verification of two universal relations for simple ionic liquids. kinetic properties of a model 2:1 molten salt, J. Phys. Chem. B 115 (2011) 4927—4938.

[18] S. Delpech, E. Merle-Locotte, D. Heuer, M. Allibert, V. Ghetta, C. Le-Brun, X. Doligez, G. Picard, Reactor physic and reprocessing scheme for innovative molten salt reactor system, J. Fluor. Chem. 130 (2009) 11—17.

[19] N. Umesaki, N. Iwamoto, Y. Tsunawaki, H. Ohno, K. Furukawa, Self-diffusion of lithium, sodium, potassium and fluorine in a molten LiF + NaF + KF eutectic mixture, J. Chem. Soc., Faraday Trans. 1: Phys. Chem. Condens. Phases 77 (1981) 169—175.

[20] A. Rudenko, A. Kataev, O. Tkacheva, Dynamic viscosity of the NaF-KF-NdF$_3$ molten system, Materials 15 (2022) 4884.

[21] W. Grimes, D. Cuneo, F. Blankenship, G. Keilholtz, et al., Fluid Fuel Reactors, Addison-Weslay Pub. Co., Geneva, 1958.

[22] K.A. Tasidou, J. Magnusson, T. Munro, M.J. Assael, Reference correlations for the viscosity of molten LiF-NaF-KF, LiF-BeF$_2$, and Li$_2$CO$_3$-Na$_2$CO$_3$-K$_2$CO$_3$, J. Phys. Chem. Ref. Data 48 (2019), 043102.

[23] M. Salanne, C. Simon, P. Turq, P.A. Madden, Heat-transport properties of molten fluorides: determination from first-principle, J. Fluor. Chem. 130 (2009) 38—44.

[24] J. Wu, J. Wang, H. Ni, G. Lu, J. Yu, Investigation of microscopic structure and ion dynamics in liquid Li(Na, K) eutectic Cl systems by molecular dynamics simulation, Appl. Sci. 8 (2018) 1874.

[25] K. Igarashi, Y. Okamoto, J. Mochinaga, H. Ohno, X-Ray diffraction study of molten eutectic LiF-NaF-KF mixture, J. Chem. SOC., Faraday Trans. 84 (1988) 4407—4415.

[26] S.T. Lam, Q.-J. Li, J. Mailoa, C. Forsberg, R. Ballinger, J. Li, The Impact of Hydrogen Valence on its Bonding and Transport in Molten Fluoride Salts, in: Electronic Supplementary Material (ESI) for J Mater Chem A, The Royal Society of Chemistry, 2021. https://www.rsc.org/suppdata/d0/ta/d0ta10576g/d0ta10576g1.pdf.

[27] B. Mignacca, G. Locatelli, Economics and finance of molten salt reactors, Prog. Nucl. Energy 129 (2020), 103503.

[28] C. Andreades, R.O. Scarlat, L. Dempsey, P. Peterson, Reheat-air Brayton combined cycle power conversion design and performance under nominal ambient conditions, J. Eng. Gas Turbines Power 136 (2014), 062001.

[29] C.W. Forsberg, Market basis for salt-cooled reactors: dispatchable heat, hydrogen, and electricity with assured peak power capacity, Nucl. Technol. 206 (2020) 1659—1685.

[30] M.M. Tylka, J.L. Willit, J. Prakash, M.A. Williamson, Method development for quantitative analysis of actinides in molten salts, J. Electrochem. Soc. 162 (2015). H625—H633.

[31] S. Sharma, A.S. Ivanov, C.J. Margulis, A Brief guide to the structure of high-temperature molten salts and key aspects making them different from their low-temperature relatives, the ionic liquids, J. Phys. Chem. B 125 (2021) 6359—6372.

[32] S.-C. Lee, Y. Zhai, Z. Li, N.P. Walter, M. Rose, B.J. Heuser, Comparative studies of the structural and transport properties of molten salt FLiNaK using the machine-learned neural network and reparametrized classical forcefields, J. Phys. Chem. B 125 (2021) 10562—10570.

[33] A.E. Galashev, V.P. Skripov, Stability of Lennard-Jones crystal structures in the molecular dynamics model, J. Struct. Chem. 26 (1985) 716—721.

[34] A.E. Galashev, V.P. Skripov, Stability and structure of a two-component crystal using a molecular dynamics model, J. Struct. Chem. 27 (1986) 407—412.